Electrolytic Extraction of Copper, Molybdenum and Rhenium from Molten Sulfide Electrolyte

Citation: Sahu, Sulata K. et al. "Electrolytic Extraction of Copper, Molybdenum and Rhenium from Molten Sulfide Electrolyte." Electrochimica Acta 243 (July 2017): 382-389. © 2017 Elsevier Ltd

As Published: http://dx.doi.org/10.1016/j.electacta.2017.04.071

Publisher: Elsevier BV

Persistent URL: https://hdl.handle.net/1721.1/131165

Version: Author's final manuscript: final author's manuscript post peer review, without publisher's formatting or copy editing

Electrolytic Extraction of Copper, Molybdenum and Rhenium from Molten Sulfide Electrolyte

Sulata K. Sahu, Brian Chmielowiec, Antoine Allanore*

Department of Materials Science and Engineering, Massachusetts Institute of Technology, Cambridge, Massachusetts 02139, USA

*: *Corresponding author, allanore@mit.edu*

Abstract

The validity of the electrochemical series for metal sulfides decomposition in their standard state has been tested experimentally at 1500 K for La_2S_3, Cu_2S, MoS_2, and ReS_2 in a molten electrolyte with the following molar composition: $(BaS)_{54}$-$(Cu_2S)_{31}$-$(La_2S_3)_{15}$ (electrolyte B). Voltammetry measurements indicated the presence of faradaic reactions in the investigated electrolyte with and without the addition of MoS_2 and/or ReS_2. Electrolysis experiments showed that the addition of La_2S_3 to BaS-Cu_2S increases the faradaic efficiency for liquid copper production with respect to a previously studied $(BaS)_{54}$-$(Cu_2S)_{46}$ electrolyte, and enabled isolation of elemental sulfur as the anodic product. Electrochemical measurements suggested the need to take into account the activity of dissolved Cu_2S in order to explain the observed cell voltage during electrolysis. Electrolysis in the presence and absence of ReS_2 and/or MoS_2 confirmed their relative stability as predicted by assuming decomposition in their standard states. Analysis of the metal products electrowon from an electrolyte containing Cu_2S, MoS_2, and ReS_2 indicates that simultaneous production of solid and liquid phases with nonequilibrium compositions.

1. **Introduction**

Copper, molybdenum, and rhenium are metals, that have found application in various fields. Copper has a wide range of applications in the electronics, building, and transportation industries because of its excellent physical properties (such as high electrical and thermal conductivity) and outstanding workability and corrosion resistance [1]. Molybdenum is frequently used as an alloying agent in steels and superalloys to enhance hardenability, strength, toughness, and corrosion resistance [2-4]. Rhenium is used as a catalyst for numerous reactions and is also added to high-temperature superalloys finding applications in jet engines [5, 6]. Molybdenum and rhenium are critical elements with low earth-abundance and are mainly obtained as by-products of copper sulfide ores mining [7, 8]. Over 90% of the world's primary copper in the earth crust is present in the form of sulfide minerals, such as chalcocite (Cu_2S), chalcopyrite ($CuFeS_2$), and bornite (Cu_5FeS_4) [9]. Per the current industrial practice, oxidation of sulfides (including iron sulfide) to form sulfur dioxide is an essential step in the production scheme of Cu, Mo and Re [10, 11]. During such operation, numerous hazardous volatile products, such as sulfur dioxide (SO_2), are produced, requiring significant additional steps and energy spending to enable compliance with environmental regulations. As a matter of fact, the existing supply chain is a net consumer of energy [10, 11], with more than 80% being in the form of electricity. In addition, the ultimate recovery of each individual metal through conventional methods involves numerous processing steps, as oxidation of sulfides exhibit limited selectivity. These makes the development of new extraction plant difficult, in part because of the corresponding capital investments [1, 12]. Therefore, there is an opportunity for new extraction processes if they can provide effective measures to solve the above issues. In particular, it is

beneficial to develop a method to capture most of the sulfur in a stable, inert, and condensed form, such as solid elemental sulfur [13].

Direct electrolysis of metal compounds into their constitutive elements is one approach that is relevant in this context [14], for example for locations where both ore and GHG-free electricity are available. In particular, electrolysis in an electrolyte of the same chemical nature as the mining feedstock that contains the multiple metals such as sulfides is of interest. In principle, electrolysis can also offer the selective recovery of multiple metals contained in the sulfides ores. Recently researchers made an effort to drive this reaction using halide melt as the electrolyte [15-18, see ref. 18 for an overview]. However, several challenges are appearing in molten salt approach [18], including the limited solubility for sulfur ion, the limited selectivity of solid-state sulfide reduction approaches and the production of solid powders. In the present work electrolytic extraction of liquid copper from Cu_2S is investigating by conducting electrolysis directly in an all-sulfide melt. To date, very little work towards the direct electrolytic reduction of sulfides in molten sulfides has been reported [18-21]. Very recently, Sokhanvaran et al [18] demonstrated the electrochemical production of liquid copper by direct electrolysis of Cu_2S in a molten sulfide electrolyte composed of 57 wt% BaS and 43 wt% Cu_2S at 1105°C (1378 K). Their results proved molten sulfides free of alkali sulfides could be used as an electrolyte to conduct faradaic reactions. This prior study showed that the faradaic efficiency as evaluated based on solid copper recovery post experiments decreased with electrolysis duration. In addition, precipitation of a barium sulfide rich phase around the cathode was reported, likely to hinder further progress of the faradaic reaction. Finally, this prior report could not isolate significant quantities of elemental sulfur as the anodic product, one of the important aspects of a direct electrolysis process for metal sulfide.

The present work pursues the electrochemical study of BaS-based electrolyte in the context of copper extraction from sulfides, with the objective to answer to several questions that arise from the prior art. The first question relates to the relationship between faradaic efficiency for copper and sulfur recovery and the amount of ionic sulfide compounds present in the melt. A full answer to such a question requires improving the knowledge of both thermodynamic and transport properties (or at least electrochemical behavior) of multicomponent mixtures of sulfides. The second question pertains to the fate of accessory metal sulfides such as molybdenum or rhenium during the electrolysis of copper sulfide. This second question also calls for the ability to predict the thermodynamic and electrochemical behavior of MoS_2 and ReS_2 in the molten sulfide electrolyte chosen for Cu_2S extraction.

Answering both questions is not possible with the existing knowledge on molten sulfides. One step forward is to verify the validity of the electrochemical series predicted from the Ellingham diagram presented in Figure 1, one of the few non-controversial thermodynamic data available for sulfides. Figure 1 is obtained using the Nernst equation, by considering the chemical reactions 1a and 2a, and their corresponding decomposition potentials 1b and 2b where M, Cu_2S, MS_2 reference states are the pure species in their stable state at temperature:

$$4Cu + S_2 = 2Cu_2S \quad (1a)$$

$$E = E^{\circ} - \frac{RT}{4F} ln\left(\frac{a^2_{Cu_2S}}{a^4_{Cu} \cdot p_{S_2}}\right) \quad (1b)$$

$$M + S_2 = MS_2 \ (M = Mo, Re) \quad (2a)$$

$$E = E^{\circ} - \frac{RT}{4F} ln\left(\frac{a_{MS_2}}{a_M \cdot p_{S_2}}\right) \quad (2b)$$

In Figure 1, the pure species are considered ($a_{Cu_2S} = a_{M_2S} = a_M = 1$) and the partial pressure of

sulfur is one atmosphere.

As a first step, the present work investigates the role of the addition of a third sulfide, lanthanum (III) sulfide (La_2S_3) to the BaS-Cu_2S electrolyte previously studied. As seen from Figure 1, pure La_2S_3 (a rare earth metal sulfide) is presumably energetically more stable than copper sulfide and barium sulfide, indicating that the selective electrochemical decomposition of Cu_2S [22, 23] following equation 1a should be possible. Furthermore, the addition of lanthanum sulfide is reported to enhance the ionic conductivity of sulfide based solid electrolytes [24]. Consequently, a pseudo ternary BaS-Cu_2S-La_2S_3 melt is anticipated to exhibit a more ionic behavior than BaS-Cu_2S. In addition, lanthanum sulfide is expected to have a low vapor pressure, allowing an extension in the range of operating temperatures of molten sulfide electrolytes. However, no ternary phase diagram involving BaS, Cu_2S, and La_2S_3 exists to date though their pseudo-binary phase diagrams have been reported [18, 25, 26]. Hence a rapid screening of some of the compositions involving BaS, Cu_2S, and La_2S_3 in the molten state near the melting temperature of copper was conducted, followed by the electrochemical study of one of the candidate (electrolyte B).

From a mining feedstock aspect, the study of the interaction of Re sulfides in different mineralogical compositions (closely associated with the formation of bornite and chalcocite) revealed that Re does not associate with any of the minerals contained in the sulfide ores [27]. More importantly, Re does not enter isomorphically into the Cu minerals; most of Re in the ore occurs as an independent sulfide $(Re,Mo)S_2$ [27]. It has been reported [28, 29] that the solubility of ReS_2 in MoS_2 is less than 20 % at 1273 K. A group of researchers [28] studied MoS_2-ReS_2 solid-state solubility and revealed that molybdenite dissolves 1 to 3 wt% Re (T = 673 K to 1273 K) whereas a much smaller amount of Mo enters ReS_2 [30]. The affinity of Re to molybdenite is

presumably inherited from the identical ionic radii of both metals. The presence of Cu and Fe may be responsible for the stable structure of the Mo–Re sulfide minerals [28]. Evaluating whether molybdenum and rhenium sulfides mined simultaneously with copper sulfides will be recovered during copper electrolysis in molten sulfide requires first an optimal process for copper extraction from its ore concentrate or matte. Nevertheless, the fact that Mo and Re sulfides are not soluble in copper sulfides minerals suggest that the Ellingham diagram reported in Figure 1 is a valuable resource to predict the behavior of these accessory metals. It shows that at any temperature, ReS_2 is energetically less stable than MoS_2, itself less stable than Cu_2S when all the compounds are pure and in equilibrium with the pure metal and $S_2(g)$. At 1500 K, the Gibbs energy of formation of ReS_2 is -16.9 kJ mol^{-1}, indicating that the decomposition of ReS_2 is close to spontaneous. It remains to be verified if using such of thermodynamic assumption in a multicomponent molten sulfide electrolyte is valid. The solution behavior of those sulfide compounds in the identified molten sulfide electrolyte remains indeed unknown. In addition, the possible alloying of the metal products (Cu, Mo and Re) during electrolysis may also alter the predictions from Figure 1. This work therefore investigates the validity of the predictions from Figure 1, including the chemical stability and electrochemical behavior of molybdenum and rhenium sulfide at 1500 K in the candidate electrolyte B.

2. Experimental

2.1. Materials and Methods

Barium sulfide (BaS, 99.7%, metals basis, Alfa Aesar), copper (I) sulfide (Cu_2S, 99.5%, metals basis, Alfa Aesar) and lanthanum (III) sulfide (La_2S_3, 99.7%, metals basis, Alfa Aesar), were used for preparation of the electrolyte. In order to obtain an electrolyte with a larger ionic transference number compared to the previously studied [18] electrolyte, $(BaS)_{54}$-$(Cu_2S)_{46}$, a significant fraction of Cu_2S was substituted by La_2S_3. Five different possible electrolyte

compositions presented as points A to E respectively in the ternary representation of Figure 2 were prepared by mixing appropriate molar ratios of starting materials in an argon atmosphere glovebox. These candidate electrolytes were heated in graphite crucibles to 1400K and 1500K and held for one hour with a minimal flow of argon (<1 cm^3 min^{-1}) before being cooled to room temperature at 10K min^{-1}. Microscopic, optical, electronic observations and compositional analysis of the solidified melt were used to evaluate melting. Pellets of MoS_2 and ReS_2 were obtained by compacting the respective powders in a hydrostatic press followed by sintering in an evacuated quartz ampoule at 973 K for two hours. The solubility of MoS_2 and ReS_2 in one selected electrolyte, (electrolyte B) was estimated by equilibrating the pellets of MoS_2 and ReS_2 with a melt at 1500 K for two hours in an argon atmosphere, followed by quenching of the sample to room temperature.

The behavior of Re and Mo sulfides in electrolyte B was investigated by adding 0.002 moles of ReS_2 (ReS_2, 99.7%, metals basis, Alfa Aesar) or/and 0.003 moles of MoS_2 (MoS_2, 99.7%, metals basis, Alfa Aesar) to electrolyte B.

2.2. Electrochemical measurements

A set of electrochemical measurements viz: open circuit potential (OCP), potentiostatic electrochemical impedance spectroscopy (EIS), cyclic voltammetry (CV), and galvanostatic and potentiostatic electrolysis were conducted. Measurements were carried out using a potentiostat/galvanostat (Reference 3000, Gamry). The OCP, EIS and CV measurements utilized a three-electrode configuration whereas a two-electrode configuration was used to conduct the electrolysis experiments. In the three-electrode configuration, the counter electrode was located at the bottom of the cell whereas the working and reference electrodes were positioned at the upper section of the cell (downward-facing working electrode). When targeting the recovery of

the cathodic products, a two-electrode set-up with the working electrode being the bottom of the graphite crucible was used (upward-facing cathode). The details of the electrochemical cell designs are available elsewhere [18]. High purity graphite (99.9995%, Alfa Aesar) was used for all electrodes for all the measurements and molybdenum wires served as the electrical leads. All the potentials in voltammetry are referred to the graphite pseudo-reference electrode and corrected post-measurements by 60% of the ohmic resistance measured between the working and reference electrodes measured at OCP using EIS. The cell voltages are also corrected by 60% of the ohmic resistance measured by EIS between the two electrodes prior to electrolysis.

The electrodes and the graphite crucible containing the electrolyte were placed in an alumina tube purged with argon at 20 cm^3 min^{-1} and the cell assembly was held in the isothermal of avertical furnace (Split Furnace MODEL: SS15R-2.50X6V-1Z, Mellen) at 1500 K. The electrodes were lowered until electrical contact with the electrolyte bath was detected. The electrochemical cell assembly was held at 1500 K for at least one hour before conducting the electrochemical measurements. The presence of faradaic reactions in the electrolyte melt was determined by cyclic voltammetry. Constant current electrolysis was carried out to evaluate the ability to extract copper from the studied electrolyte containing: a) 54BaS - 31Cu_2S - 15La_2S_3 (electrolyte B) b) electrolyte B with 0.003 mol MoS_2 (4 mol %), c) electrolyte B with 0.002 mol ReS_2 (3 mol %), and d) electrolyte B with 0.003 mol MoS_2 (4 mol %) and 0.003 mol ReS_2 (3 mol %). The faradaic efficiency for both potentiostatic and galvanostatic electrolysis was evaluated by comparing the estimated amount of solidified copper present in or near the cathode, compared with Faraday's law for cuprous ion (Cu^+) reduction.

2.3. Characterization and analysis

The solidified samples were observed by an optical microscope (Olympus BX51, Olympus) after metallurgical preparation described in [18]. Microstructure of the electrolyte before and after electrochemical measurements was observed and analyzed by a scanning electrode microscope (SEM, JEOL JSM-6610LV, JEOL Ltd.) equipped with an Energy Dispersion Spectroscopy analyser (EDS, Sirius SD detector, SGX Sensortech Ltd.) for elemental analysis. The compositions of the metallic products were verified after carbon coating of the samples, using wavelength dispersive electron microprobe analysis (WDS) with a JEOL-JXA-8200 Superprobe (JEOL Ltd.) instrument operated at an accelerating voltage of 15 kV, a beam current of 20 nA, and a beam size of 1µm. Pure Re, Mo, and Cu metal standards were used for calibration of the probe. The solidified electrolytes (before or after the electrolysis) as well as the collected anodic and cathodic products were characterized by X-ray diffraction spectroscopy after crushing. Powder X-ray diffraction (XRD) patterns were collected using a PANalytical X'pert PRO XRPD (Cu K_α radiation). Data were recorded from 10 to 70° (2θ) at a step size of 0.02° (2θ) and a collection time of 2 seconds per step. For phase identification, PANalytical Highscore Plus software, PDF file version 3.0, was used. Process efficiency was estimated by weighing the recovered copper using a scale (Sartorius, 0.001 g accuracy), and normalizing by the theoretical amount of copper that should be produced from the charges passed, assuming a one-electron transfer process.

3. Results

3.1. Electrolyte composition

Though the pseudo-binary phase relations involving BaS, Cu_2S, and La_2S_3 are reported [18, 25, 26], no pseudo-ternary phase diagram are available. Hence selection of an appropriate composition consisting of BaS, Cu_2S, and La_2S_3, which essentially need to be molten at 1500 K

remains empirical. The selected electrolyte compositions presented in Figure 2 were melted at 1400 K and 1500 K. Compositions A to C proved molten at 1400K and all five compositions (A to E) proved molten at 1500 K. Extrapolating from the La_2S_3-Cu_2S and La_2S_3-BaS phase diagrams, an increase in lanthanum sulfide concentration lead to an increase in the liquidus temperature, suggesting the possible formation of ternary and/or quaternary high melting lanthanum rich phases. Hence, further electrochemical studies where limited to the electrolyte 54BaS - 31Cu_2S - 15La_2S_3 (electrolyte B) at 1500 K. The microscopic, optical, and electronic observations and compositional analysis of the solidified electrolyte B after dissolution experiments of MoS_2 and ReS_2 pellets at 1500 K indicated that about 0.01wt% of MoS_2 dissolves in two hours, whereas ReS_2 does not dissolve appreciably (below WDS detection limit). Electrolyte B with 0.002 moles of MoS_2 is therefore expected to be saturated in dissolved Mo^{4+}, and the equivalent cations concentrations viz; Ba^{2+}, Cu^{+}, La^{3+}, Mo^{4+} are expected be 12.90 mol L^{-1}, 14.62 mol L^{-1}, 3.65 mol L^{-1} and 0.01 mol L^{-1} respectively.

3.2. Cyclic voltammetry measurements in electrolyte B

Figure 3 displays the second cycle of DC cyclic voltammograms recorded at a scan-rate of 5 $mV \cdot s^{-1}$ on a graphite electrode in electrolyte B at 1500 K, in the absence or presence of MoS_2 and/or ReS_2. The decreased in the solution resistance at OCP measured in the presence of MoS_2 along with the shape of the cyclic voltammogram in Figure 3b may indicate an increase of the electronic conductivity under such conditions. However, the simultaneous presence of solid (MoS_2) and molten semiconducting phases (Ba_xCu_yS liquid), along with the uncertainty in the mechanism of electronic conduction in molten sulfides, limit the ability to further assess the role of electronic conduction on the observed electrochemical signals. Figure 3a shows the forward and reverse scans for electrolyte B with a concentration of Cu^{+} at 14.62 mol L^{-1}. For the forward

scan and potential sweep from 0.400 V to -0.400 V, the corresponding change in current density at the working electrode varies from 18 A cm^{-2} to -12.5 A cm^{-2}. At the most positive potentials, very large anodic currents are measured, with jittering most likely due to rapid fluctuations in the solution resistance. This is typical of gas evolution in melts at high temperature. As the potential is scanned toward negative potentials, a sharp increase in current (magnitude) is observed. The current crosses zero at approximately 0.05 V, until a current plateau at -0.75 A cm^{-2} is observed in the potential range 0.000 V to -0.200 V. The current increases at -0.200 V indicates the start of a second reduction reaction, whose current increases sharply with potential and this second reduction reaction corresponds to reduction of cuprous ion to metallic copper. This sharp increase stops at the initiation of the reverse scan at -0.400 V, leading to a plateau in the backward scan at around -12.5 A·cm^{-2}, transforming to a wave at around -0.200 V. The presence of a larger cathodic current on the backward scan in the range -0.400 to 0.000 V has been reproducibly observed across cycles and experiments, and is attributed to the interaction between the metal product (liquid copper, see electrolysis results hereafter, often sticks to the graphite electrolyte and grows during the cathodic cycle, leading to a larger electrode surface area) and the graphite working electrode. An anodic plateau at around 2.5 A cm^{-2} is observed from -0.050 V to 0.400 V. An abrupt rise in the anodic current is observed upon the potential returning to 0.400 V, characteristic of a wall, attributed to the oxidation of sulfide ions as validated by the electrolysis results presented hereafter.

Figures 3b to 3d present the second cycle of voltammograms recorded in electrolyte B in the presence of MoS_2 (Figure 3b), ReS_2 (Figure 3c) and both MoS_2 and ReS_2 (Figure 3d). According to the study of the solubility experiment reported above, MoS_2 in both experiments is above saturation with a concentration of dissolved Mo ions at 0.01 mol·L^{-1} meaning that a

significant fraction (~ 99%) of MoS_2 is present as solid particles at the investigated composition. Figure 3b also exhibits an anodic current wall in the most positive potential regions of the scan, albeit at a less positive potential and with smaller current density than in absence of MoS_2 (Figure 3a). The cathodic current starts very close to 0.000 V, leading to a plateau at less negative potentials than in absence of MoS_2, at -0.175V and -5 A cm^{-2}. A change in slope is observed around -0.200 V, with discontinuous signal jumps observed for potentials more negative than this value. On the backward scan, the current in the cathodic region is less than on the forward scan, crossing zero at -0.125 V. The results in the presence of MoS_2 show a reproducible additional cathodic event closer to 0.000 V that reduces the window of potential between the anodic wall and the large cathodic currents reported in the absence of MoS_2 beyond -0.200 V. Electrolysis results (see next section) will show that indeed molybdenum is the cathodic product in the selected electrolyte B and concentration of MoS_2.

Even though the appearance of the cyclic voltammogram for electrolyte B in the presence of ReS_2 (Figure 3c) is similar to the one observed for electrolyte B (Figure 3a), the cathodic current does not increase during the backward scan. Additionally, there are two potential cross-overs in Figure 3a, which is not the case for electrolyte B in the presence of ReS_2 (Figure 3c). ReS_2 is barely soluble in electrolyte B, and is present as solid particles in the fully molten electrolyte B at the beginning of an experiment. The anodic current wall is observed in a similar range of potential (around 0.400 V) as in the absence of ReS_2, the only noticeable difference being the presence of an anodic current plateau starting at around 0.200 V and 2.5 A cm^{-2} on the forward sweep which gradually decreases as the potential becomes negative eventually crossing the zero current line at -0.125V. For potentials more negative, a sharp decrease in current is observed at -0.300 V leading to a current plateau at -17 A cm^{-2}. On the backward scan, the

plateau is not observed and the cathodic currents decrease steadily until -0.200 V, after which a small current plateau is observed at -1.25 A·cm^{-2}. The current becomes anodic beyond 0.080 V, gradually reaching the anodic wall observed again at 0.400 V. The overall potential window and the points of zero current are therefore not much different from what is observed in the absence of ReS_2 (see Figure 3a), and electrolysis results will indeed show (see next section) the production of both copper and rhenium.

The cyclic voltammogram for electrolyte B in presence of both ReS_2 and MoS_2 (Figure 3d) appears to exhibit appreciable redox waves, not present in the other conditions (Figure 3a to 3c). Such feature of Figure 3d can be attributed to the presence of larger total concentration of MoS_2 and ReS_2. As seen from Figure 3d, the anodic portion of the sweep exhibits a monotonic current increase, reproduced in both the forward and backward scan. The zero current is measured reproducibly at 0.000 V, and the monotonic anodic behaviour is characteristic of a resistance. The cathodic current shows a plateau reached at -0.300 V and around -13 A cm^{-2} on the forward scan, and a gradual reduction to a wave-like current at -0.220 V and -2.5 A cm^{-2}. This plateau joins the monotonic current potential behaviour at around 0.000 V. Electrolysis results showed that the three metals (Cu, Re, Mo) are obtained as cathodic products at large current densities, with significant interaction between all three species.

3.3. Electrolysis of electrolyte B

Both galvanostatic and potentiostatic experiments were conducted at 1500 K in electrolyte B. The variation of the cell voltage during galvanostatic electrolysis at a cathodic current density of 11 A cm^{-2} using a downward-facing cathode configuration is presented in Figure 4. The cell voltage during electrolysis is larger than 0.400V during the first 15 minutes of

electrolysis. Examination after electrolysis experiments reveals the presence of shiny orange colored droplets next to the working electrode, confirmed to be copper with purity >99.4 % as measured by EDS analysis. As a complement, potentiostatic experiment at an applied cell voltage of 0.6 V was conducted for 30 minutes with an upward-facing cathode configuration where the bottom of the graphite crucible acted as the cathode. Gas evolution near the anode was visible in the optical micrograph in the form of large voids near the anode or entrapped in the bulk electrolyte, and a yellowish powder next to the anode was recovered (see Figure 5a). XRD and EDS analysis of the powder indicates pure elemental sulfur. As presented in Figure 5b, the cell exhibited an orange colored layer of 1 mm thickness at the bottom of the graphite crucible, and a color gradient gradually diminishing towards the electrolyte surface. XRD analysis of the layer indicates a mixture of phases identified as elemental Cu, elemental S, BaS, $BaCu_2S_2$ and La_2BaS_4. SEM and EDS analysis presented in Figure 5b show a relatively large concentration (approximately 50% by volume) of fine copper droplets surrounded by a copper-deficient electrolyte. Fine sulfur grains are visible on the surface of the copper droplets cross-sections via SEM-EDS as shown in Figure 5a. EDX data and image analysis of the SEM cross-section of the copper-rich layer located at the bottom of the graphite crucible indicated the presence of around 50% by volume of copper droplets. As the manual separation of these fine copper droplets is challenging, the estimated volume of copper (50%vol. at a density 8.96 g. cm^{-3} at 298 K) compared with the volume of the layer (around 0.2 cm^3; 1.6 cm diameter, 0.1 cm height) lead an estimated amount of copper of around 0.9 g. With a charge passed of 2340 coulombs, the estimated Faradaic efficiency exceeded 50% (59%), twice as larger than reported in 54BaS-46 Cu_2S [18].

3.4. Electrolysis of electrolyte B in presence of MoS_2

Galvanostatic electrolysis using a downward-facing working electrode with the addition of MoS_2 was carried out at a current density of 11 A cm^{-2}. The corresponding cell voltage shown in Figure 4b stays between 0.350 to 0.400 V, with very little variation. A layer of electro-deposited metal powders (of ~10 μm, see Figure 6) is observed surrounding the working electrode after electrolysis. Wavelength dispersive spectroscopy, though challenging due to the comparable sizes of the beam and the particles, determined that the powder was composed of molybdenum.

3.5. Electrolysis of electrolyte B in presence of ReS_2

The variation of the cell voltage during galvanostatic electrolysis of electrolyte in presence of ReS_2 at 1500 K with a cathode current density of around 11 A cm^{-2} using vertical downward-facing working electrode is displayed in Figure 4c. The cell voltage initially spike to 1.200V before rapidly decreasing for 2 minutes to about 0.600V. After a brief plateau the cell voltage slowly decreases to a steady state value of 0.250 V after 20 minutes. Optical microscope observations after electrolysis reveal shiny orange colored droplets next to the working electrode. SEM observation presented in Figure 7, and EDS analysis confirm the presence of metallic copper next to the working electrode. In addition, rhenium powder is found at the bottom of the electrochemical cell. The immiscibility of rhenium in liquid copper and its large density (21.02 $g.cm^{-3}$) help explain the location of the Re powders.

3.6. Electrolysis of electrolyte B in presence of ReS_2 and MoS_2

Galvanostatic electrolysis with a downward-facing cathode was conducted at a current density of 11 A cm^{-2} at 1500 K in electrolyte B with additions of MoS_2 and ReS_2. The corresponding cell voltage, shown in Figure 4d, starts at around 0.600 V and gradually decreases to 0.250V after

1200 seconds. The cell voltage was greater than 0.400 V for more than half of the time. Optical microscope observations again revealed the presence of shiny orange colored droplets next to the working electrode. Figure 8 shows that molybdenum and rhenium grains are found dispersed in the copper metal matrix as observed with SEM and analyzed with EDS. The results of WDS analysis averaging ten different points per phase are reported in Table 1. Inclusions of trace amounts of barium and sulfur impurities were found. The observed dark matrix of Figure 8 is metallic copper with purity >99%, with traces of molybdenum, sulfur, and barium ($Cu_{99.15}Mo_{0.02}Ba_{0.22}S_{0.611}$). The brightest phase is predominantly rhenium, with an average composition of $Re_{80.71}Cu_{12.87}Mo_{3.66}Ba_{0.18}S_{1.06}$, which translates into $Re_{84.11}Cu_{12.07}Mo_{3.87}S_{0.28}$ assuming the 2% barium is present as BaS impurity. The last phase of grey color in Figure 8 was found to be predominantly molybdenum, at a composition of $Mo_{73.27}Cu_{16.38}Re_{3.37}Ba_{0.09}S_{6.26}$ measured by WDS. Taking into account the solubility of sulfur in molybdenum [31], and assuming the remaining sulfur is associated to Cu and Ba, the recalculated composition is found to be $Mo_{96.88}Cu_{1.05}Re_{2.08}S_{3.88}$.

4. Discussion

The results of both dynamic (cyclic voltammetry) and static (constant current and constant potential) measurements with electrolyte B confirmed the electrochemical series as computed in conventional Ellingham diagram (Figure 1) for La_2S_3, BaS, and Cu_2S. Copper metal was the only metal deposited as a result of electrolysis. The addition of La_2S_3 leads to larger (+50% vs +28%) estimated Faradaic efficiency for metallic copper than in 54BaS-46 Cu_2S. This confirms that rare-earth metal sulphides act as more ionic compounds than Cu_2S in the molten state, in agreement with predictions from solid-state knowledge. The present study has isolated the anodic product and confirmed the production of elemental sulfur for the first

time, confirming an important feature of the direct electrolysis of metal sulfide in molten sulfides.

The detailed analysis of the features observed on the cyclic voltammetry (Figure 3a) is beyond the scope of the present work, but the potential difference between the wall of sulfur evolution and the most cathodic limiting plateau indicates a decomposition voltage of at least 0.6V for electrolyte B, a value confirmed by galvanostatic measurements (Figure 4a). This value is around 200mV larger than the one anticipated from Figure 1. Taking into account the nonstandard state of Cu_2S in electrolyte B by replacing the activity of Cu_2S in equation 1b with its concentration (ideal behavior) predicts a shift of the decomposition potential of 100mV, suggesting a negative deviation from ideality for Cu_2S in BaS (i.e an activity coefficient lower than unity for Cu_2S).

The relative stability of molybdenum, rhenium, and copper sulfides according to Figure 1 is also confirmed by the results of our electrochemical experiments in electrolyte B. Rhenium sulfide is not significantly soluble in electrolyte B, and rhenium metal does not alloy appreciably with copper. The stability of ReS_2 therefore follows the predictions from Figure 1, which states a nearly spontaneous decomposition at 1500K. This is confirmed by our results, which always showed production of Re when ReS_2 was present (results from Figure 3c and 4c), although no clear electrochemical signals inherited from the reduction of ReS_2 could be identified in the present study. The corresponding absence of remaining ReS_2 in the electrolyte after electrolysis confirmed its decomposition.

MoS_2 was found to decompose to Mo upon electrolysis in electrolyte B. Saturation of the electrolyte with MoS_2 (with residual solid MoS_2 present) lead to a significant modification of the electrochemical response in the cyclic voltammetry conditions studied in this work (Figure 3b),

and likely affected the conductivity of electrolyte B. Nevertheless, the electrochemical 'window' for electrolyte B in the presence of MoS_2 is reduced to around 0.4V as confirmed by the galvanostatic measurements (Figure 4b). A selective decomposition of MoS_2 with respect to Cu_2S was observed experimentally at around 0.4V, in reasonable agreement with the prediction from Figure 1. It remains to be demonstrated how much of the current passed in Figure 4b has actually been used for Mo production, since electronic conduction may become important in the presence of un-dissolved MoS_2.

The simultaneous extraction of Cu, Mo, and Re in electrolyte B (Figure 3d and 4d, Figure 8 and Table 1) at high current density is again in agreement with Figure 1, though the metallurgy of the cathode products suggests some deviation from standard decomposition potentials.

Concerning the liquid copper product, the presence of sulfur and molybdenum (see Figure 8, Table 1) is in agreement with the reported literature data [31] which suggest solubility of 0.01% and 0.1%, respectively. The rhenium powder had a low copper content as the two metals are virtually immiscible, even at very high temperature [31]. Therefore rhenium grains are formed in the liquid copper cathode (Figure 8). Only 4% of Mo is found in the Re grains, half of solubility reported in prior study [31], which indicated around 8% of molybdenum solubility in solid rhenium up to 1500 K. Molybdenum grains had a very small copper content, though the presence of a surrounding copper matrix lead to some interference in WDS analysis. The rhenium content in the molybdenum grains is around 2 %, again lower than literature predictions which anticipate as much as 20% of Re solubility in solid Mo.

The lack of saturation of both the rhenium and molybdenum grains observed in the present work may be inherited from a density-driven segregation that can happen in liquid copper during electrolysis, since rhenium is twice as dense as molybdenum. This finding suggests using a liquid

cathode product (here copper) as a host may enable separation of ancillary elements (here Mo and Re) that may be co-reduced along the main metal, because of their presence in the feedstock ore. Validation of the concept with actual ore concentrate is necessary as the thermodynamic state of Mo, Re and Cu in actual sulfide ores, where iron sulfide is present as a key coexisting phase, is likely different from the pure sulfide powders used in the present study.

5. Conclusions

Electrolytic extraction of copper, molybdenum, and rhenium was conducted successfully at 1500 K using an electrolyte composed of alkaline-earth, rare-earth, and copper sulfides. The addition of a rare-earth metal sulfide component to the electrolyte increased the faradaic efficiency and the recovery/isolation of sulfur as the anodic product. The electrochemical series calculated from the standard state was confirmed for La_2S_3, Cu_2S, MoS_2 and ReS_2, though care must be taken to account for the solution behavior of the species. ReS_2 reduction is near spontaneous and the selective reduction of MoS_2 proved possible. The simultaneous presence of Cu_2S, MoS_2, and ReS_2 lead to the production of phase separated solid grains of Mo and Re included in liquid copper. Both solid phases had not reached saturation in each other.

Acknowledgments

The authors acknowledge Norco Conservation and the Office of Naval Research (contract N00014-12-1-0521) for their financial support to this project. The geological and thermodynamic insight into the mineralogy of Mo- and Re- bearing copper sulfide ores provided by Dr. Marcelo de Oliveira is greatly appreciated.

References

[1] R. Kerr, The coming copper peak. Science, 343 (2014) 722.

[2] Y. Jiraskova, J. Bursik, M. Hapla, I. Turek, Influence of molybdenum on the alloying and physical properties of Fe-Al. J. Supercond. Novel Magn. 28 (2015) 905.

[3] B. Hu, Q. Cai, H. Wu, Influence of Mo on growth and coarsening of nanometer-sized carbides in low-alloy ferritic steels containing Ti. J. Iron Steel Res. Int. 21 (2014) 878.

[4] B. Han, Y. Ma, H. Peng, L. Zheng, H. Guo, Effect of Mo, Ta, and Re on high-temperature oxidation behavior of minor Hf doped β-NiAl alloy. Corros. Sci. 102 (2016) 222.

[5] B. Bryskin, J. Carlen, Rhenium and molybdenum/tungsten based alloys: an overview of database. (Minerals, Metals & Materials Society) (1998) pp 11-37.

[6] G. Du, M Abu-Omar, Oxo and imido complexes of rhenium and molybdenum in catalytic reductions. Curr. Org. Chem. 12 (2008) 1185.

[7] A. V. Elutin, M. V. Istrashkina, Z. A. Peredereeva, Rhenium recovery from secondary raw materials of various types. (Minerals, Metals & Materials Society), (1997) pp 135-139.

[8] E. Peters, Direct leaching of sulfides: chemistry and applications, Metall. Trans., B 7B (1976) 505.

[9] D. Dreisinger, Copper leaching from primary sulfides: Options for biological and chemical extraction of copper. Hydrometallurgy 83 (2006) 10.

[10] R. P. Nardi, Extractive metallurgy of copper. Copper production with growth potential. Metal. Mater. 62 (2006) 344.

[11] J. W. Matousek, Sulfur in copper smelting slags, in: Proceedings of the Copper 95--Cobre 95 International Conference, Santiago, Nov. 26-29, 1995, p 531.

[12] M. E. Schlesinger, M. J. King, K. C. Sole, W. I. G. Davenport, Extractive Metallurgy of Copper, Elsevier, Amsterdam, 2011.

[13] F. Habashi, Extractive metallurgy of copper, Int. J. Miner. Process. 46 (1996) 295.

[14] A. Allanore, Contribution of Electricity to Materials Processing: Historical and Current Perspectives. JOM 65(2) (2013) 130.

[15]. T. Wang, H. Gao, X. Jin, H. Chen, J. Peng, G. Z. Chen, Electrolysis of solid metal sulfide to metal and sulfur in molten NaCl–KCl, Electrochem. Comm. 13(2011) 1492.

[16]. M. Tan, R. He, Y. Yuan, Z. Wang, X. Jin, Electrochemical sulfur removal from calcopyrite in molten NaCk-KCl, Electrochimica Acta 213 (2016) 148.

[17]. H. Gao, M. Tan, L. Rong, Z. Wang, J. Peng, X. Jin and G. Z. Chena, Preparation of Mo nanopowders through electroreduction of solid MoS_2 in molten KCl–NaCl, Phys. Chem. Chem. Phys., 16 (2014) 19514.

[18] S. Sokhanvaran, S. K. Lee, G. Lambotte, A. Allanore, Electrochemistry of Molten Sulfides: Copper Extraction from BaS-Cu_2S, J. Electrochem. Soc. 163(2016) D115.

[19] X. L. Ge, S. Seetharaman, The salt extraction process - a novel route for metal extraction part 2 - Cu/Fe extraction from copper oxide and sulphides. Trans. Inst. Min. Metall., Sect. C 119 (2010) 93.

[20] X. Ge, X. Wang, S. Seetharaman, Copper extraction from copper ore by electro-reduction in molten $CaCl_2$-NaCl. Electrochim. Acta 54 (2009) 4397.

[21] T. Biegler, D. C. Constable, Continuous electrolytic reduction of a chalcopyrite slurry. J. Appl. Electrochem. 7 (1977) 175-179.

[22] D. R. Stull, H. Prophet, JANAF Thermochemical Tables (NSRDS-NBS 37). 2nd ed National Standard Reference Data system, 1971.

[23] D. R. Gaskell, Introduction to Metallurgical Thermodynamics. 2nd Ed , Hemisphere Publ. Corp., Michigan, 1981.

[24] Z. Liu, Y. Tang, X. Lu, G. Ren, F. Huang, Enhanced ionic conductivity of sulfide-based solid electrolyte by incorporating lanthanum sulfide, Ceram. Int. 40 (2014) 15497.

[25] N. V. Sikerina, O. V. Andreev, Phase equilibria in the systems SrS-Cu_2S-Ln_2S_3 (Ln = La or Nd). Zh. Neorg. Khim. 52 (2007) 665.

[26] O. V. Andreev, P. V. Miodushevscy, R. Serlenga, N. N. Parsukov, Phase equilibria in the BaS-Ln_2S_3 systems. J. Phase Equilib. Diffus. 26 (2005) 109.

[27] A. B. Yusupova, Study of Dzhezkazgan rhenium-bearing ore by chemical phase analysis, "Nauka" Kaz. SSR, 1970, p 124.

[28] M. Drabek, M. Rieder, V. Bohmova, The Re-Mo-S system: new data on phase relations between 400°C and 1200°C. Eur. J. Mineral. 22 (2010) 479.

[29] V. I. Rekharskii, L. V. Savel'eva, A. I. Gorshkov, Y. P. Dikov, A. P. Zhukhlistov, N. V. Trubkin, A. F. Fedotov, A. I. Tsepin, Phase relations in the system molybdenum disulfide-rhenium disulfide (according to experimental data), Izv. Akad. Nauk SSSR, Ser. Geol, (1983) 86.

[30] Y. Takahashi, An atomic level study of rhenium and radiogenic osmium in molybdenite. Geochim. Cosmochim., Acta 71 (2007) 5180.

[31] L. Kaufman, User applications of alloy phase diagrams, Proceedings of an international conference on user applications of alloy phase diagrams, American Society for Metals, 1987.

Figure Captions

Figure 1: The Ellingham diagram for BaS, La_2S_3, Cu_2S, MoS_2 and ReS_2. At 1500 K, the decomposition potentials (ΔE^0) for ReS_2, MoS_2 and Cu_2S are 0.06 V, 0.33 V, and 0.45 V, respectively.

Figure 2: Possible electrolyte compositions, $0.54BaS - (0.46\text{-}x)\ Cu_2S - xLa_2S_3$ (x = 0.15 to 0.35) presented in $BaS\text{-}Cu_2S\text{-}La_2S_3$ ternary diagram at 1500 K. The selected electrolyte composition is $0.54BaS - 0.31Cu_2S - 0.15La_2S_3$, (electrolyte B). The pseudo-binary system involving $BaS\text{-}Cu_2S$, $Cu_2S\text{-}La_2S_3$ and $La_2S_3\text{-}BaS$ at 1500 K are projected along the axes of the ternary diagram and the ternary compounds presented across the pseudo-binary line do not necessarily exist at 1500 K. The ternary compounds found at lower temperature are in parenthesis. For $BaS\text{-}Cu_2S$, the compounds $BaCu_2S_2$, $BaCu_4S_3$ do not exist at this temperature and a liquid phase involving BaS and Cu_2S appears for X_{Cu2S} = 0 to 0.65. The dotted line represents the liquidus. Along the $Cu_2S\text{-}La_2S_3$ cross-section, $CuLa_2S_4$ coexists with γ phase of La_2S_3 and liquid Cu_2S. In $La_2S_3\text{-}BaS$ system, at 1500 K, solid solution of BaS in La_2S_3 (γ phase) has been reported over the composition range X_{La2S3} = 0.56 to 1. La_2BaS_4 does not exists at this temperature.

Figure 3: DC cyclic voltammetry at a scan-rate of 5 $mV.s^{-1}$ and 1500 K, measured in **(a)** electrolyte B, **(b)** electrolyte B + 4 mol% $MoS_{2(solid)}$, **(c)** electrolyte B + 3 mol% $ReS_{2(solid)}$ and **(d)** electrolyte B + 4 mol% of $MoS_{2(solid)}$ + 3 mol% of $ReS_{2(solid)}$. The solution resistances for figure (**a**) to (**d**) are 1.4 Ω, 0.3 Ω, 0.6 Ω, and 0.2 Ω respectively.

Figure 4: Variation of the cell voltage (ΔE) during galvanostatic electrolysis at a cathode current density of 11 A cm^{-2} during 30 minutes at 1500 K, in **(a)** electrolyte B, **(b)** electrolyte B with 4 mol% MoS_2 powders, **(c)** electrolyte B with 3 mol% of ReS_2 powders and **(d)** electrolyte B + 4 mol% of MoS_2 + 3 mol% of ReS_2 powders. The solution resistances for figure (**a**) to (**d**) are 1.2 Ω, 0.3 Ω, 0.5 Ω, and 0.3 Ω respectively.

Figure 5: **(a)** Optical (inset) and SEM analysis of the collected yellow powder as the anode product after the potentiostatic electrolysis of electrolyte B at 1500 K. **(b).** Optical (inset) and SEM image of a half-cell and the solidified electrolyte after potentiostatic electrolysis in electrolyte B at 1500 K. EDS is used to determine compositions.

Figure 6: Back-scattered image and EDS analysis results of the solidified electrolyte B with 0.003 moles of MoS_2 after electrolysis at a cathode current density of 11 A cm^{-2} for 30 minutes at 1500 K.

Figure 7: Back-scattered image and EDS analysis results of the solidified electrolyte B with 0.003 moles of ReS_2 after electrolysis at a cathode current density of 11 A cm^{-2} for 30 minutes at 1500 K.

Figure 8: Back-scattered image and EDS analysis results of the cathodic product after electrolysis in electrolyte B with 0.003 moles of MoS_2 and 0.002 moles of ReS_2 at a cathode current density of 11 A cm^{-2} for 30 minutes at 1500 K.

Fig 1

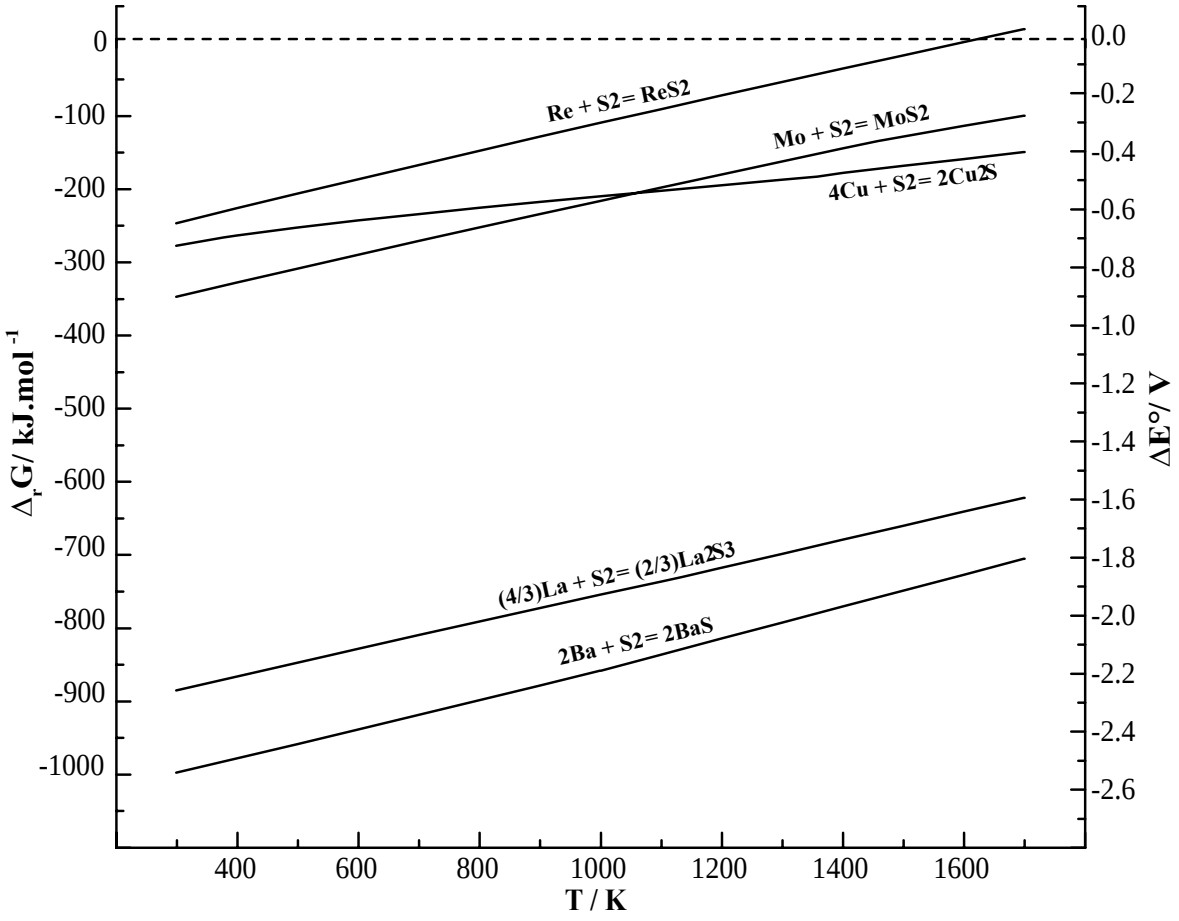
Re + S2= ReS2
Mo + S2= MoS2
4Cu + S2= 2Cu2S
(4/3)La + S2= (2/3)La2S3
2Ba + S2= 2BaS
ΔrG/ kJ.mol-1
ΔE°/ V
T / K
0
-100
-200
-300
-400
-500
-600
-700
-800
-900
-1000
0.0
-0.2
-0.4
-0.6
-0.8
-1.0
-1.2
-1.4
-1.6
-1.8
-2.0
-2.2
-2.4
-2.6
400
600
800
1000
1200
1400
1600

Fig 2

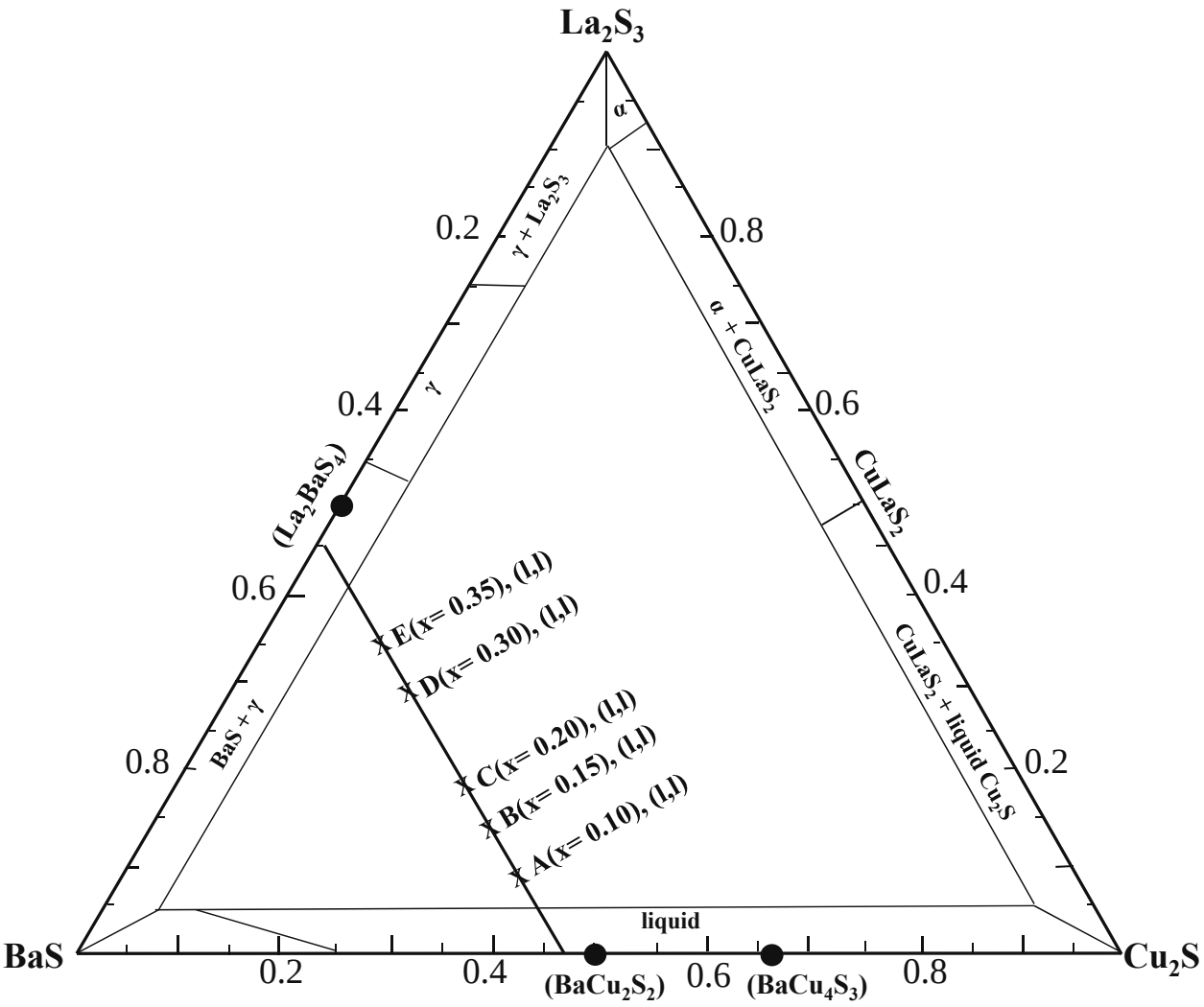
La2S3
α
γ + La2S3
α + CuLaS2
γ
(La2BaS4)
CuLaS2
E(x= 0.35), (l,l)
D(x= 0.30), (l,l)
C(x= 0.20), (l,l)
B(x= 0.15), (l,l)
A(x= 0.10), (l,l)
BaS + γ
CuLaS2 + liquid Cu2S
liquid
BaS
(BaCu2S2)
(BaCu4S3)
Cu2S
0.2
0.4
0.6
0.8

Fig 3

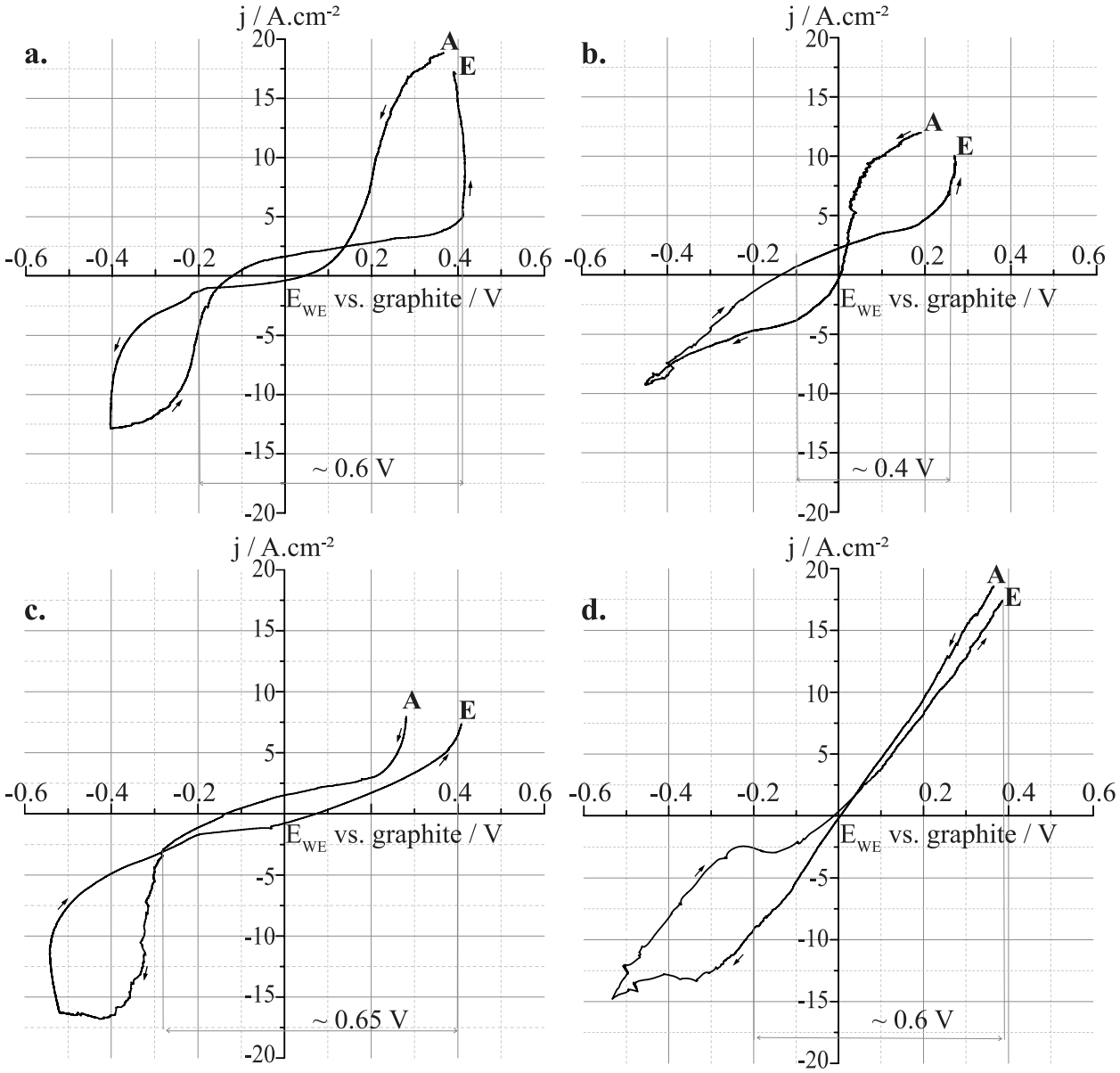

Fig 4

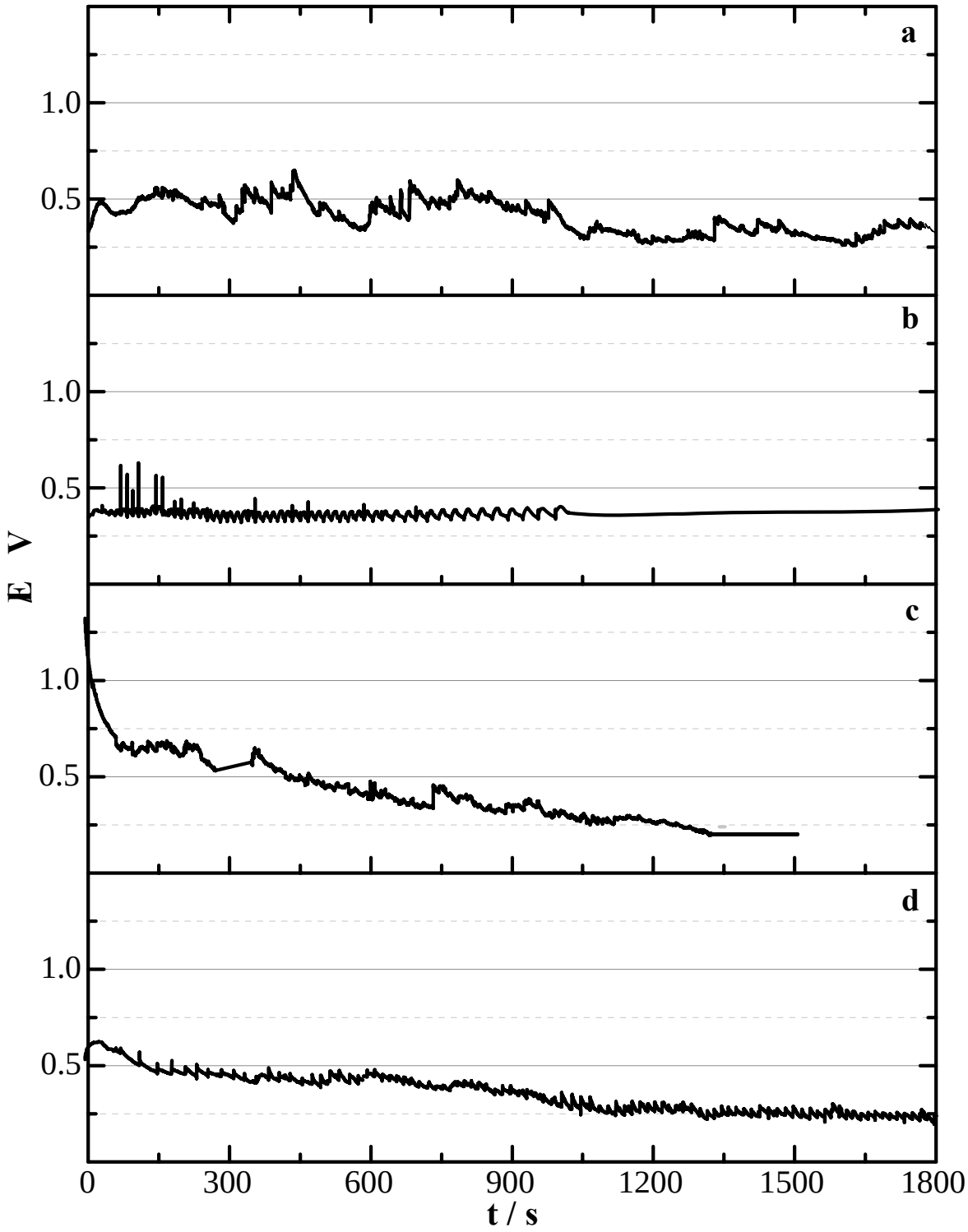

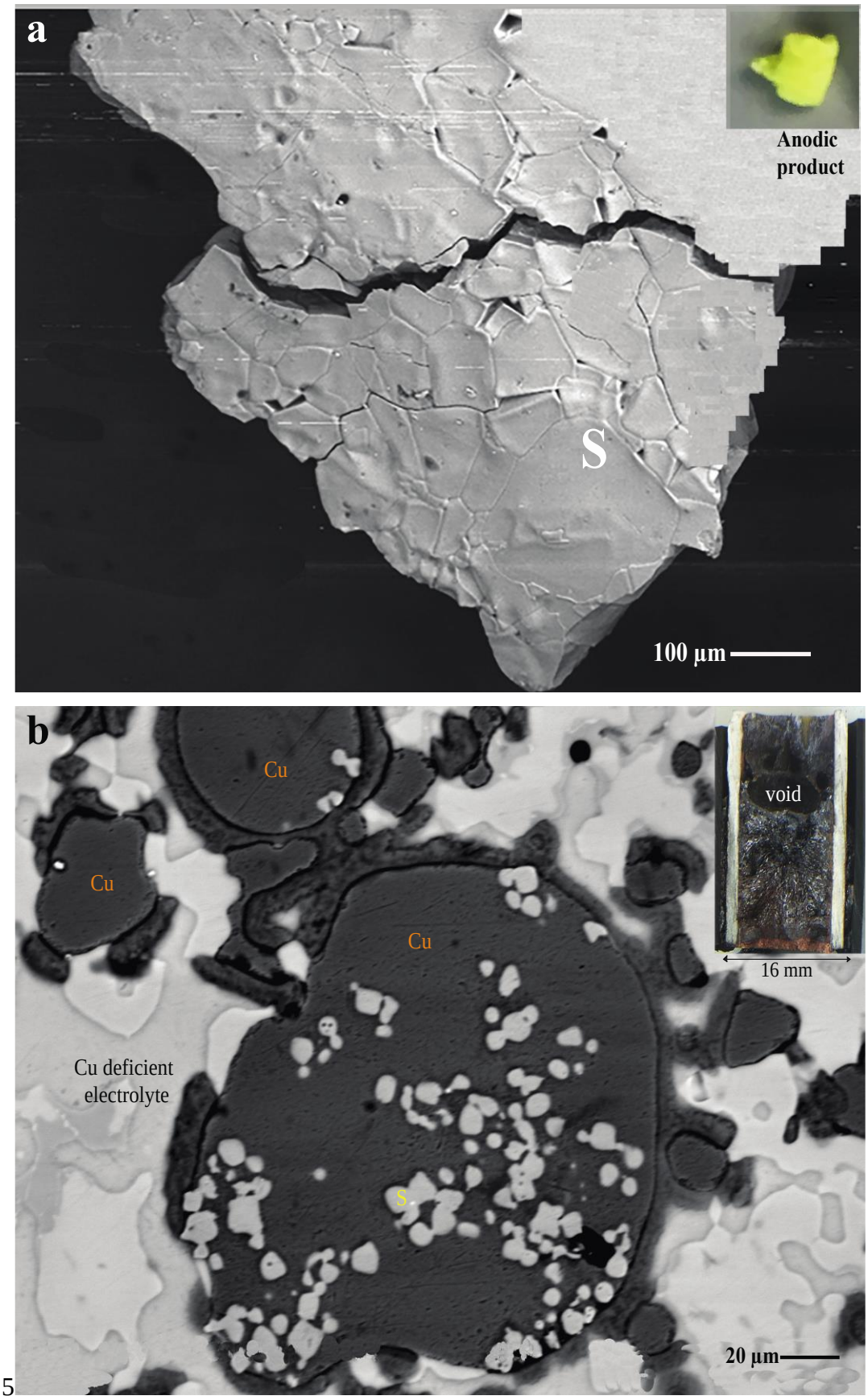
a
Anodic
product
S
100 µm
b
Cu
Cu
Cu
Cu deficient
electrolyte
S
void
16 mm
20 µm

Fig 5

Fig 6

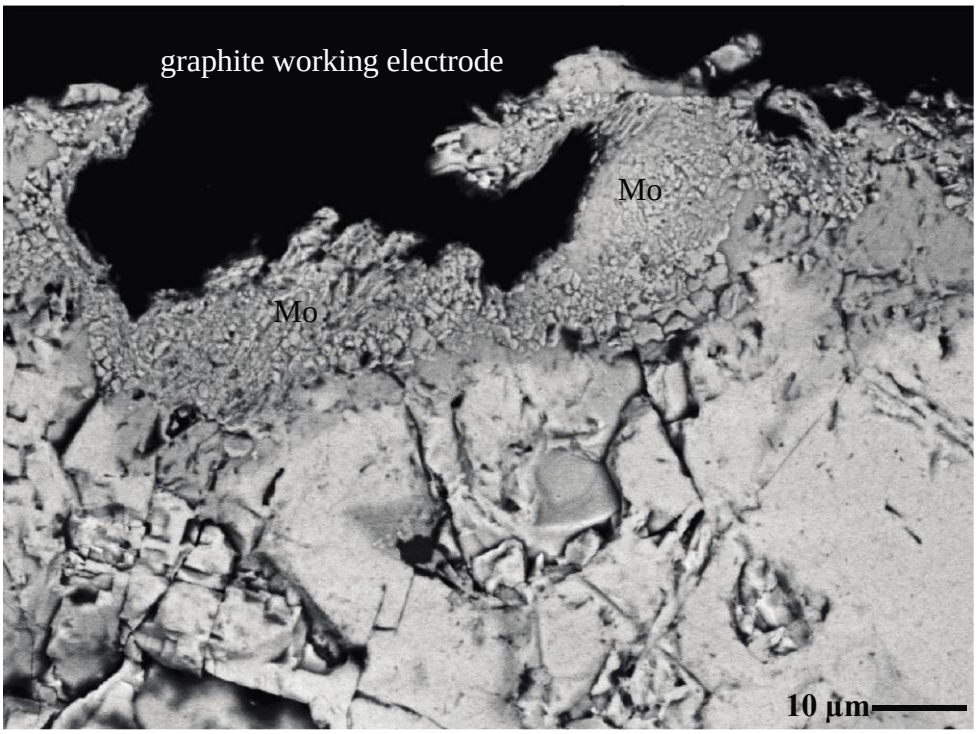

Fig 7

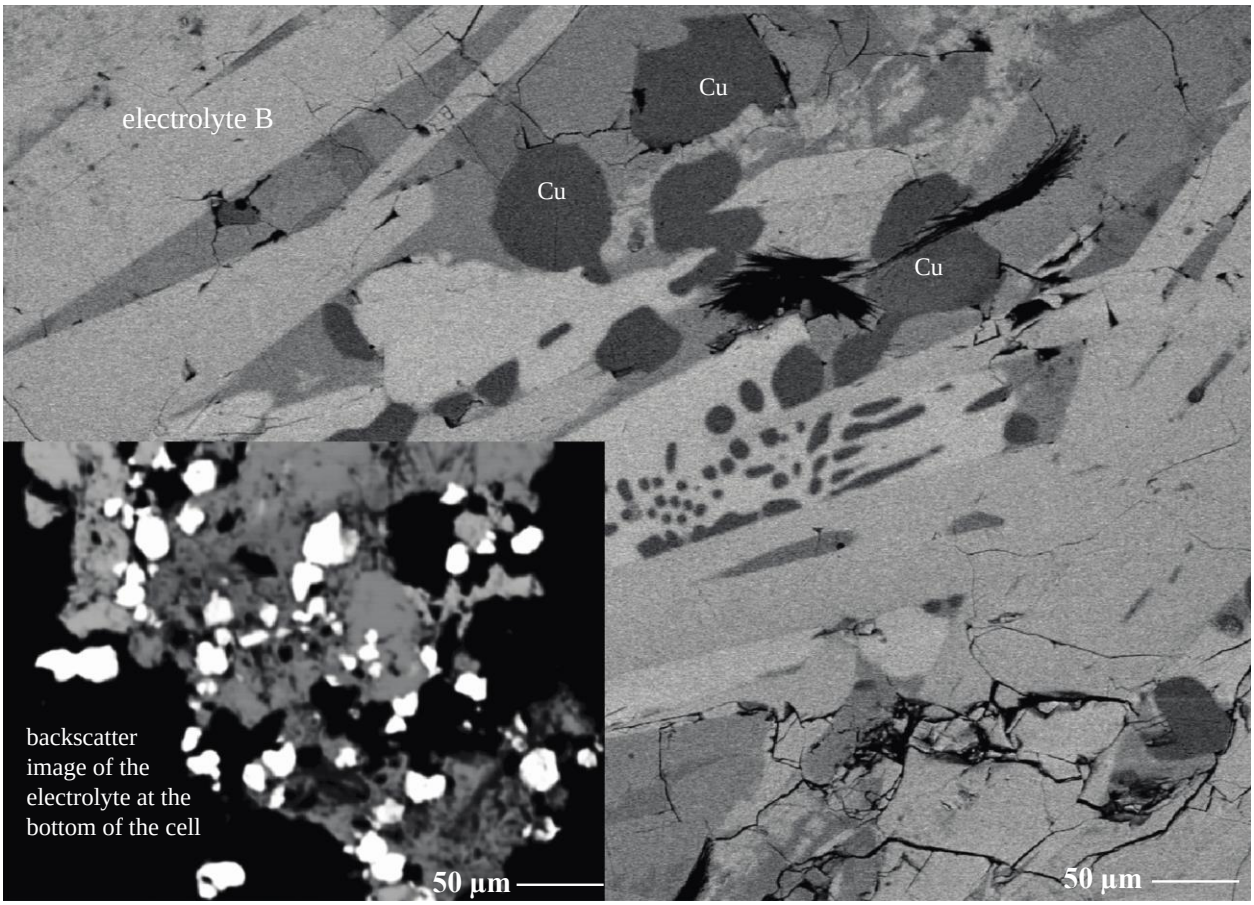
electrolyte B
Cu
Cu
Cu
backscatter image of the electrolyte at the bottom of the cell
50 µm
50 µm

Fig 8

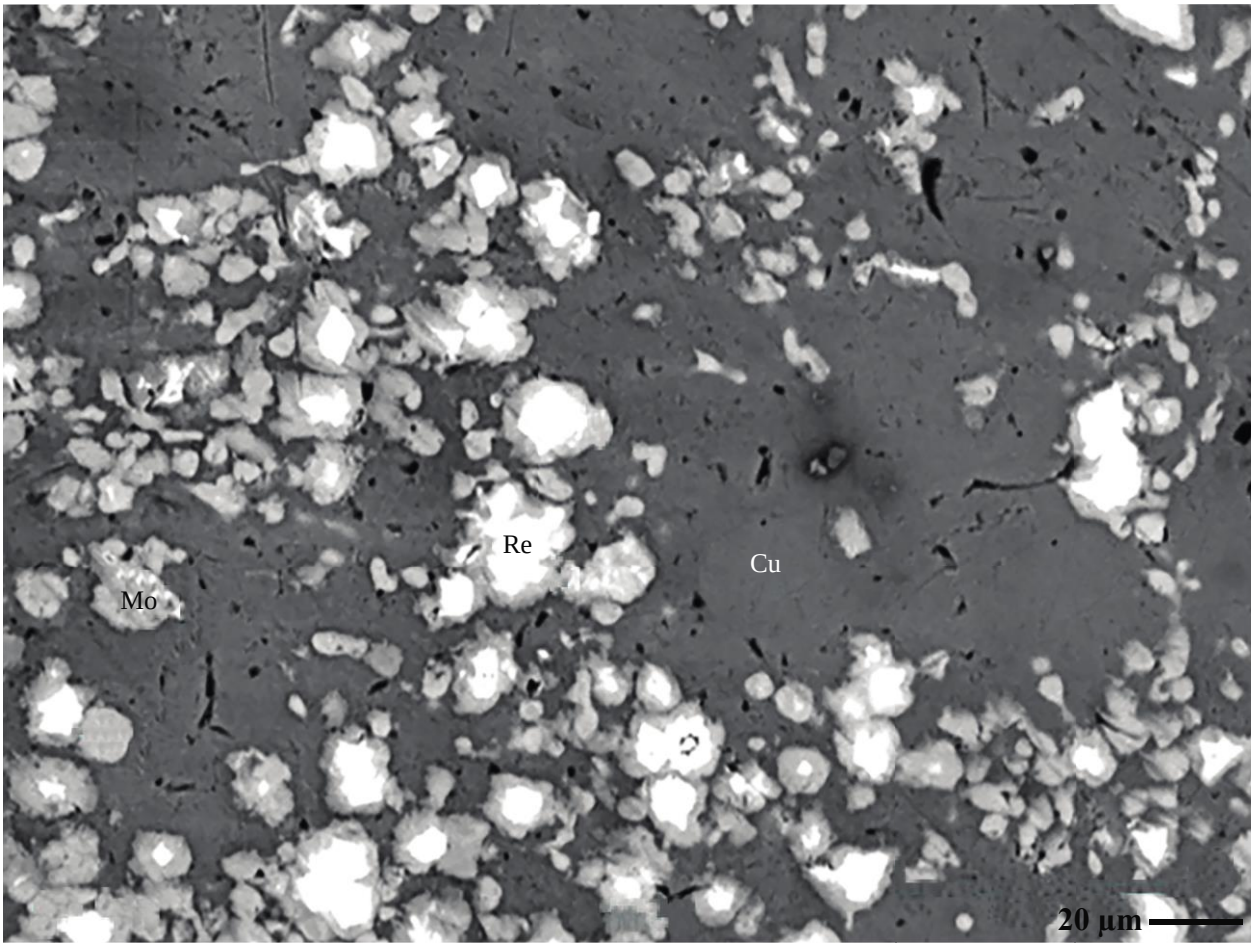

Table 1: Microprobe chemical analysis of the cathodic product after electrolysis of electrolyte B in presence of MoS_2, ReS_2 (Fig. 4d).

Analysis from Figure 8	**Compositions**
Dark	$Cu_{99.15}Mo_{0.02}Ba_{0.22}S_{0.61}$
Intermediate	$Cu_{16.38}Re_{3.37}Mo_{73.27}Ba_{0.09}S_{6.26}$ $Cu_{1.05}Re_{2.08}Mo_{96.88}S_{3.88}$
Bright	$Cu_{12.87}Re_{80.71}Mo_{3.66}Ba_{0.18}S_{1.06}$ $Cu_{12.07}Re_{84.11}Mo_{3.87}S_{0.28}$